Modifying the STM Tip for the 'Ultimate' Imaging of the Si(111)-7×7 Surface and Metal-supported Molecules

Ye-liang Wang*, Zhi-hai Cheng, Zhi-tao Deng, Hai-ming Guo, Shi-xuan Du, and Hong-jun Gao*

Abstract: We report on high-resolution STM measurements with modified probe tips. First, both the rest atoms and adatoms of a Si(111)-7×7 surface are observed simultaneously. The visibility of rest atoms is dependent upon the sample bias voltage (less than –0.7 V) and is enhanced by sharpening the tip, which is rationalized by first-principles calculations. Second, a tip with a perylene molecule adsorbed at its apex is used to discriminate the molecular states and the metal states of the underlying Ag(110) surface, which is attributable to a mismatch between the energy levels of the functionalized tip and the adsorbates on silver. Lastly, high-resolution images of iron phthalocyanine (FePc) and zinc phthalocyanine (ZnPc) molecules on Au(111) are obtained by using an O_2-terminated tip, and the images reveal rich intramolecular features arising from molecular orbitals that are not observed when using clean metallic tips.

Keywords: High resolution · Molecule · Si(111)-7×7 · STM · Tip

1. Introduction

Over the past three decades, the scanning tunneling microscope (STM) has proven to be one of the most powerful modern research tools, enabling investigations of the morphology and local properties of solid surfaces. Its capacity for high spatial resolution was firstly demonstrated by measurements of reconstructed semiconductor surfaces. The gain of unprecedented images in real space is still stimulating studies based on semiconductors, which usually have complicated geometric reconstruction and intricate electronic structures.[1]

Besides semiconductor surfaces, STM also holds remarkable potential for the imaging and spectroscopy of adsorbed molecules on well-defined metal surfaces. In the past several decades, various organic–inorganic interfaces have been extensively investigated with the aim to construct molecular-based functional nanodevices.[2–9] Besides the observations of geometric superstructures in different dimensions[6,8,10–21] or the configuration of individual molecules in self-assemblies,[22–25] researchers are seeking to explore molecular electronic structures with higher resolution, allowing direct imaging of intrinsic molecular orbitals and further providing a deeper understanding of the molecule–substrate interaction. The majority of STM studies of individual molecules have so far been limited to molecules on metal or semiconductor substrates, since STM relies on nonzero conductance within the tunneling junction to produce an image. In these cases, the electronic structure of the molecules is usually influenced by the substrate.[26] This limitation could be overcome by decoupling molecules from the substrate, for example, by using an ultra thin insulating inorganic film[27] or a molecular buffer layer between molecular adsorbates and a metal substrate.[26,28,29]

An alternative way to get high-resolution images is to functionalize the STM tip by attaching a molecule at its apex.[30–32] Every STM event is a convolution of tip and sample structures and thus the electronic structure of the tip affects the capability of STM imaging. A functionalized tip with CO or C_2H_4 has been found to increase the resolution of STM imaging of small molecules.[32,33] However, for large molecules less work has been done on directly measuring the molecular electronic structures in detail.

In this review paper, we first show the highest resolution STM images to date of the (7×7) reconstruction of the silicon(111) surface by a tip with a quite tiny apex. We then demonstrate that the electronic structures of metal-supported molecules can be directly imaged by molecule-terminated STM tips. Functionalizing the tip by attaching a molecule (either a solid perylene molecule or O_2 gas molecule) to its apex is expected to modify the tip's electronic structure. With the functionalized tips, STM images of molecules on metal reveal intramolecular features not observed with normal metallic tips. The functionalization of a metal tip could be a useful method for increasing the resolution of molecules adsorbed on metal surfaces or even for discriminating electronic states of organic adsorbates and states of the metal surfaces.

2. 'Ultimate' STM Images of the Si(111)-7×7 Surface

The Si(111)-7×7 surface is a best friend of the STM community and is inseparable from the history of STM. This surface holds the most complicated and fascinating reconstruction in several stacked atomic layers and provides a platform for testing the unprecedented resolution of STM as a novel powerful apparatus.[34] The first real-space atomic image of this surface was obtained by Binnig *et al.* in their landmark STM demonstration, in which bright spots corresponding to the topmost adatoms were revealed.[35] Since then, with STM and the later family of scanning probe microscopes, the structures of the Si(111)-

Correspondence: Prof. H.-j. Gao, Prof. Y.-l. Wang
Chinese Academy of Sciences,
Institute of Physics,
Beijing 100190, China
Tel.: +86 10 82648035
Fax: +86 10 62556598
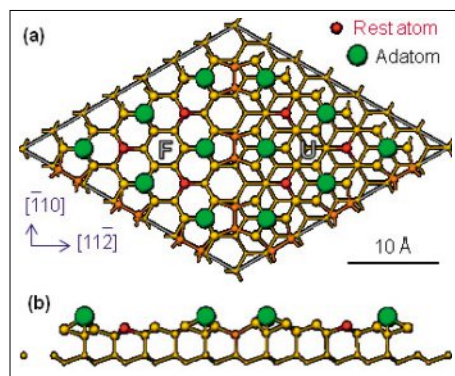E-mail: hjgao@iphy.ac.cn, ylwang@iphy.ac.cn

Fig. 1. Schematic diagram of Si(111)-7×7 'DAS' model. (a) Top view and (b) side view of atoms in Si(111) layers, the atoms at increasing depth in the surface are indicated by spots of decreasing sizes. All twelve adatoms are colored in green and all six rest atoms in red in one unit cell, which consist of two halves, a faulted half unit cell (F) and an unfaulted half unit cell (U).

7×7 surface have been extensively investigated.[36–39] The STM topographies normally show the topmost adatoms. For the mapping of rest atoms, little work has been reported that employs a common STM tip. Sutter *et al*.[39] selectively mapped the rest atoms with a semiconductor tip, since the energy gap of the tip can suppress the tunneling from the adatoms at certain sample bias voltage settings.

The atomic arrangement of the Si(111)-7×7 reconstruction is described by the DAS (dimer-adatom-stacking fault) model.[40] The model (Fig. 1) consists of twelve adatoms and six rest atoms in one unit cell, which are evenly distributed in the faulted half unit cell (FHUC) and unfaulted half unit cell (UHUC). Each unit cell contains nineteen dangling bonds (DBs), twelve for the adatoms and six for rest atoms and one for the corner atom. The tunneling current in STM of this surface originates from these DBs.

The electronic states of DBs of the adatoms is about 0.4 eV below the Fermi energy (E_F) and the states of DBs of the rest atoms is about 0.8 eV below E_F.[41] STM is very sensitive to states closest to the sample E_F, so the mapping of rest atoms, whose DBs states are far from E_F, is difficult to carry out. This is also assumed to be the main reason that adatoms and rest atoms of Si(111)-7×7 surface are difficult to clearly distinguish simultaneously. We recently revisited this surface employing a sharp STM tip.[42,43] The resulting images clearly show all adatoms and all rest atoms with high contrast. Careful preparation of the STM tips (reducing the radius of the apex) is the key to this success, as our first-principles calculations reveal a geometric hindrance effect of the apex for such complex surfaces with multiple stacked layers.

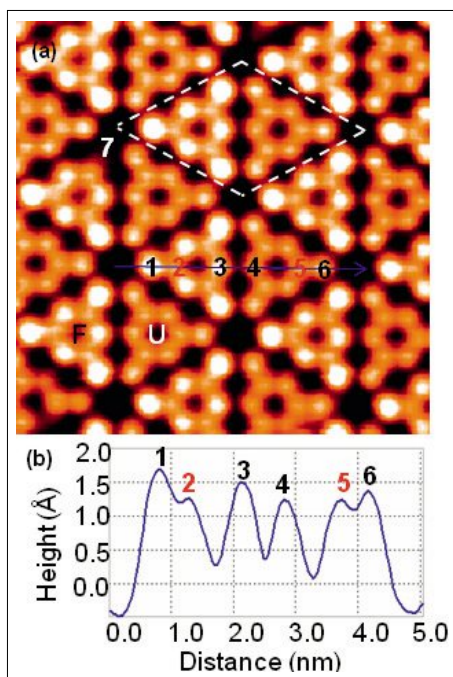The STM images in Fig. 2a clearly show the adatoms and the rest atoms, that

Fig. 2. STM images of Si(111)-7×7 surface, simultaneously revealing twelve adatoms and six rest atoms per unit cell. (a) Filled states image (8 nm × 8 nm) recorded at sample bias voltage of –1.5 V and tunneling current of 0.3 nA. A (7×7) unit cell is delineated with a dashed-line rhombus. (b) Line profile taken along the blue line in (a), with labels '1', '2', '3' denoting the corner adatom, rest atom, center adatom in faulted half unit (FHUC), and labels '4', '5', '6' denoting the center adatom, rest atom, corner adatom in unfaulted half unit (UHUC), respectively. Label '7' denotes the site where an adatom is missing.

is, 18 topographic maxima in per (7×7) unit cell. In the UHUC, the rest atoms even appear with almost the same brightness as the central adatoms, whereas in the FHUC, the rest atoms appear considerably less bright than the central adatoms. Note the defect with the missing of one corner adatom (labeled as 7) in Fig. 2a: it shows no influence

on its adjacent rest atom, and the rest atom is still visible and locates at its normal position with no lateral displacement.

The line profile in Fig. 2b shows the positions and height differences of the six distinct types of atoms (labeled as 1 to 6) along the solid line in Fig. 2a. The rest atom (site 2) in the FHUC is at the same apparent height as the rest atom (site 5) in the UHUC, and they are both even at the same height as the central adatom (site 4) in the UHUC. The high-contrast between the rest atoms and adatoms is even better than in the previous results obtained by using scanning force microscopes, in which the tip touched the silicon atoms of the substrate.[37,38,44] To our best knowledge, this is the first time that all the rest atoms and adatoms of Si(111)-7×7 surface are simultaneously revealed with high-contrast in an STM topographic image.

A series of STM images obtained at different sample bias voltages (U), as shown in Fig. 3, illustrate that the detection of rest atoms is dependent on the sample bias voltage applied. At lower bias voltage of U = –0.5 V and –0.6 V, the images (Fig. 3a and 3b) only show adatoms. This suggests the electronic states of adatoms are closer to Fermi level than are those of the rest atoms. The invisibility of the rest atoms is ascribed to the electronic states of the rest atoms being outside the range of the bias when the sample bias is kept very low. By increasing the bias voltage, the rest atom spots become visible at U < –0.7 V, as shown in Fig. 3c–f. It clearly reveals that the DB states of the rest atoms are about 0.7 eV below the E_F, which is in excellent agreement with the experimental results measured by the method of current imaging tunneling spectroscopy (CITS). In 1989, Hamers *et al.* provided CITS data of the DB states of adatoms (about 0.35 eV below the E_F) and rest atoms (about 0.8 eV below the E_F).[41]
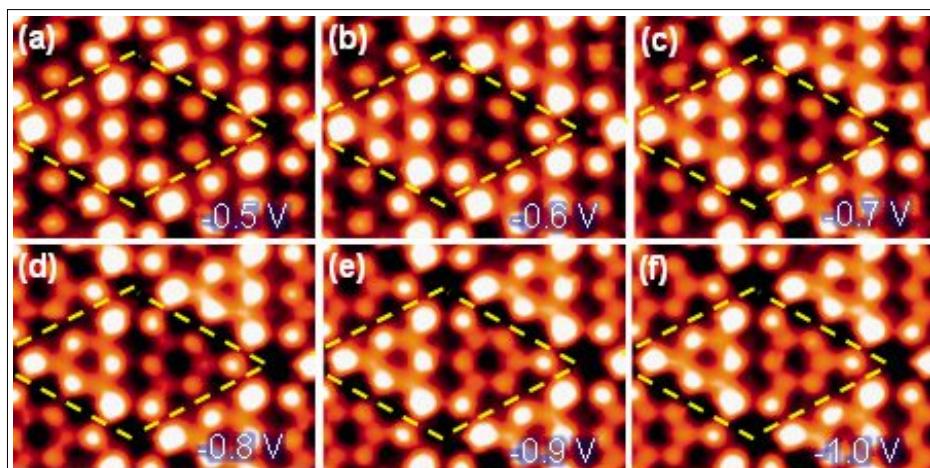

Fig. 3. STM images of Si (111)-7×7 surface with different sample bias voltages (U): (a) –0.5 V; (b) –0.6 V; (c) –0.7 V; (d) –0.8 V; (e) –0.9 V; (f) –1.0 V, respectively. The rest atoms start to appear at the sample voltages and become highly visible while U is less than –0.7 V. All images are taken at I = 0.4 nA in a scanning area of 5 nm × 5 nm.

The STM observations presented here contrast sharply with previous STM studies, which in most cases showed images similar to Fig. 4a with 12 protrusions in each (7×7) unit cell, irrespective of the bias voltages (somewhere between –2 V to 2 V). A common explanation[45] for the absence of the rest atom spots in the images relies on the fact that the tunneling probability depends on the thickness of the tunneling barrier. Because the tunneling current is inversely proportional to the exponential of the thickness, the lower electronic state locating in the valence band corresponds to the smaller tunneling current. The invisibility of rest atoms while adatoms are visible may be due to the former having significantly lower electronic states than the latter. This argument, however, contradicts the theoretical prediction that the DB states of the rest atoms extend into the vacuum region like the adatoms.[46] Also, because the rest atoms are about 4.6 Å away from the nearest adatoms, if one has an infinitely sharp tip positioned right above the rest atom, there is no reason to believe that the adatoms screen the rest-atom tunneling. If the tunneling current from a rest atom were indeed weak, one could move the tip closer to the surface (region of rest atoms) in a constant current STM mode.

The simultaneous visibility of rest atoms and adatoms has been further rationalized by theoretical simulations.[42] Fig. 4a shows the STM image of the Si(111)-7×7 surface at U = –0.57 V. At this low sample bias, the electronic states of the rest atoms are outside the range of the bias. Thus, the STM topography here reveals only the topmost adatoms. The adatoms in the FHUC appear noticeably brighter than those in the UHUC. In each half, the adatoms at the corners appear also slightly brighter than those near the center. These qualitative features are in good agreement with the calculated real-space charge distribution at this particular bias (Fig. 4b). Fig. 4c shows the STM image at U = –1.5 V. We can clearly

see both the adatoms and the rest atoms. On the UHUC, the rest atoms appear with almost the same brightness as the central adatoms, whereas on the FUHC, the rest atoms appear considerably less bright than the central adatoms. Once again, the STM observations are in excellent agreement with the calculated real-space charge distribution at the experimental bias in Fig. 4d. Tips with different apex size are used in the simulations, collectively indicating that the attainable size of the tip apex is the crucial factor in imaging the true charge distribution of a (7×7) surface.[42] The calculated result with a tip radius of 7 Å is in quantitative agreement with experimental observations (Fig. 4c and 4d).

To sum up, we have shown, by calculation and experiment, voltage-dependent charge distributions of the Si(111)-7×7 surface, and we achieved STM images that simultaneously represent both the adatoms and rest atoms. The appearance of rest atoms is dependent on the bias voltage. The rest atom spots can be visible as protrusions at the sample bias voltage less than –0.7 V. The first-principles electronic structure calculations also show a strong dependence of the charge distribution on the bias voltage: twelve spots at –0.57 V for the twelve adatoms, but eighteen spots at –1.5 V for the twelve adatoms plus six rest atoms. Our results suggest that a geometric hindrance due to the finite size of the tip apex could be the reason. This finding should arouse significant research interest in the fabrication of the STM tip and its applications in exploring more detailed information about surface reconstructions and nanostructures.

3. See the Atoms in Molecule-covered Metal Lattices by a Molecule-terminated Tip

A functionalized tip provides a possibility to image molecular electronic struc-

tures with higher resolution. The STM tip would be functionalized by approaching the tip to the sample surface with an overlayer of molecules. If the interaction of the molecules with the underlying substrate is weak, it will be favorable for a tip to pick up a molecule from the sample surface at high current setups. For example, in the case of perylene molecules at Ag(110) surface, the isolated distribution of perylene molecules on the substrate at low molecular coverage suggests a weak intermolecular interaction.[47] The theoretical calculations further confirm the weak interactions between molecule and the Ag(110) substrate.[48] The adsorption energy of a single perylene molecule on Ag(110) is about –4.5 eV. However, the adsorption energy of perylene on a tungsten tip is higher than –8.0 eV, calculated from the adsorption on a flat tungsten (100) surface. Thus the higher adsorption energy of perylene with tungsten makes it feasible for a tungsten tip to pick up molecule from the silver substrate. Therefore, a tungsten tip can be functionalized by adsorbing a perylene molecule at its apex. We modify the tip by applying voltage pulses from the tungsten tip to molecules on the sample. The STM images change to a different mode, confirming the adsorption of a perylene molecule at the tip.

With a clean tungsten tip, the perylene molecules on Ag(110) are imaged as protrusions on the surface.[48] Fig. 5a shows a high-resolution STM image of a perylene
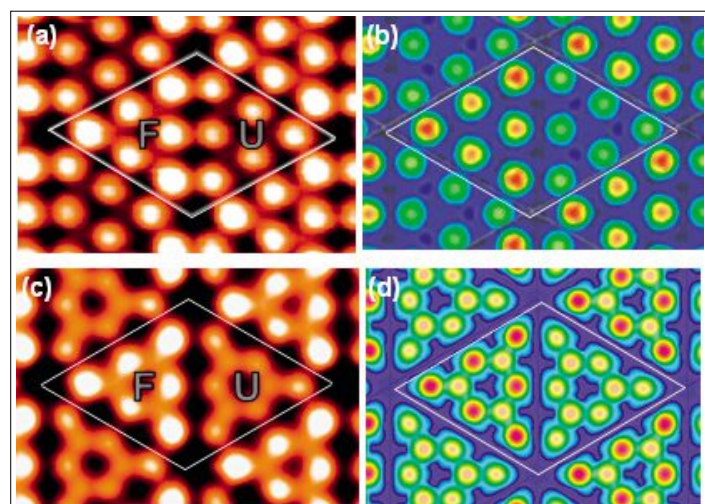
Fig. 4. (a), (c) Experimental STM images with bias voltages of –0.57 V and –1.5 V, and tunneling currents of 0.3 and 0.41 nA, respectively. F and U depict the FHUC and UHUC, respectively. (b), (d) Calculated STM images for Si(111)-7×7 with bias voltages of –0.57 and –1.5 V, respectively. The red peaks are about 2 Å above the dark blue borderlines.
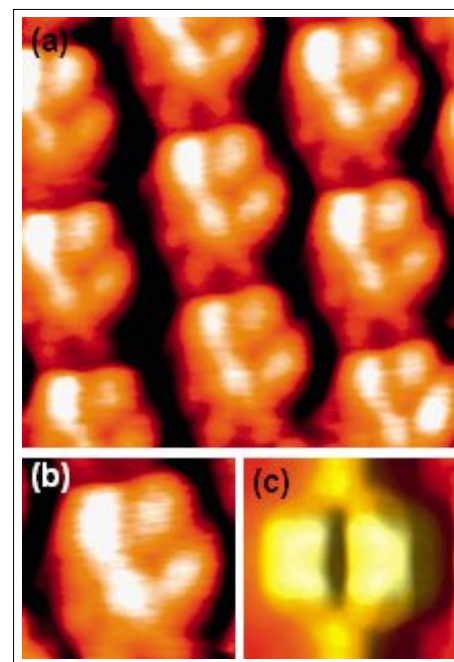
Fig. 5. STM images of a monolayer of perylene molecules self-assembled at Ag(110) surface with a clean tungsten tip. (a) A high-resolution image in scanning area of 3 nm × 3 nm. (b) Enlarged image of one perylene molecule, 1.2 nm × 1.2 nm. (c) Simulated image of one perylene molecule (1.8 V, 0.09 nA).
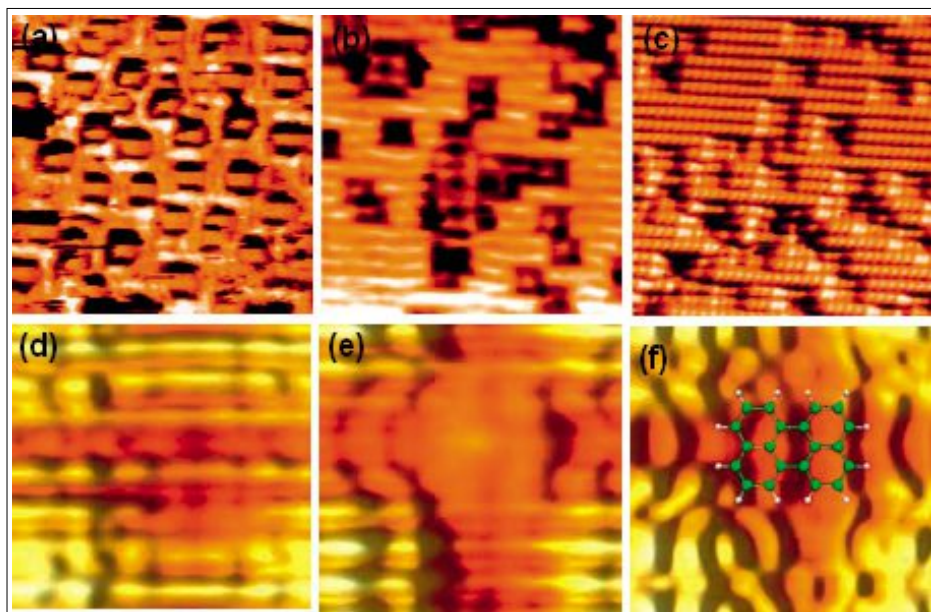
Fig. 6. (a)–(c) STM images of perylene molecules adsorbed on Ag(110) with a perylene-terminated tungsten tip. (d)–(f) STM simulations and high-resolution details of a single feature. The position of the perylene molecule on the substrate lattice is indicated in (f). Parameters: (a) 10 nm × 10 nm, 0.8 V, 27.5 pA; (b) 7.9 nm × 7.9 nm, 0.67 V, 161.5 pA; (c) 10 nm × 10 nm, 1.5 V, 149 pA.

monolayer on the Ag(110) surface. Each perylene molecule is imaged as four bright lobes with an apparent height of 1.5 Å. DFT simulations indicate that this image is mainly attributable to the π states of the molecule. The twist of the molecule in the experimental STM image is probably due to the lateral intermolecular interactions of close-packed perylene adsorbates. In a close-packed configuration, the interaction between the hydrogen atoms of adjacent molecules is the main component in the energetic stability of the molecular layer. A twist of the carbon–hydrogen bonds in this case will distort the π bonds of the molecule. Since molecule is imaged mainly *via* π states, the molecule itself may appear twisted. Comparing the experimental data in Fig. 5b with the simulation in Fig. 5c, it can be seen that the simulated STM image with a clean tungsten tip is roughly equivalent to the local charge density – *i.e.* the π states – of perylene molecules on Ag(110) surface.

With a functionalized tip, we gain much higher resolution data with intramolecular features, as shown in Fig. 6a (bias voltage –0.8 V). The energy levels of perylene adsorbates are discriminated by changing the bias voltage and current. Part of the Ag surface appears as a protrusion, and the perylene molecules appear to be embedded in the substrate. While increasing the bias voltage to –0.67 V, the whole Ag surface appears, and an image of Ag rows in the [1-10] direction is obtained (Fig. 6b). If the bias voltage is further increased to –1.5 V, a high-resolution atomic image of the Ag surface is visible while the perylene adsorbates are seen as depressions (Fig. 6c). STM simulations under identical tunneling conditions are shown in Figs. 6d–f. All features are reproduced in simulations with a perylene-modified tungsten tip.

The central part of the molecule is still visible in Fig. 6b, while it has vanished in Fig. 6c. The reason for this behavior is the onset of the *d* band on the silver surface, which reaches its maximum density of states at around –1.5 eV. At a bias of –1.5 V, the protrusion in the middle of the molecule no longer appears, and the STM images reveal only the atomic positions of the silver surface. The observations clearly demonstrate the induced functionality of the tip due to the adsorbed molecule. While the states of the molecule at the surface are invisible due to their increased energy difference from the states of the tip, the continuous *d* band of Ag(110) gradually provides the majority of tunneling electrons around –1.5 eV.

We also note that varying the adsorption geometry of perylene on the tungsten tip, *e.g.* by rotating the molecule or changing its adsorption site, does not affect the results of the STM simulations. This indicates that most of the tunneling current is transported from the attached perylene molecule, while the influence of the tungsten tip configuration is rather small. To understand the nature of this intriguing effect in depth, we performed a partial charge density calculation for a perylene molecule on a W(100) film.[49] The
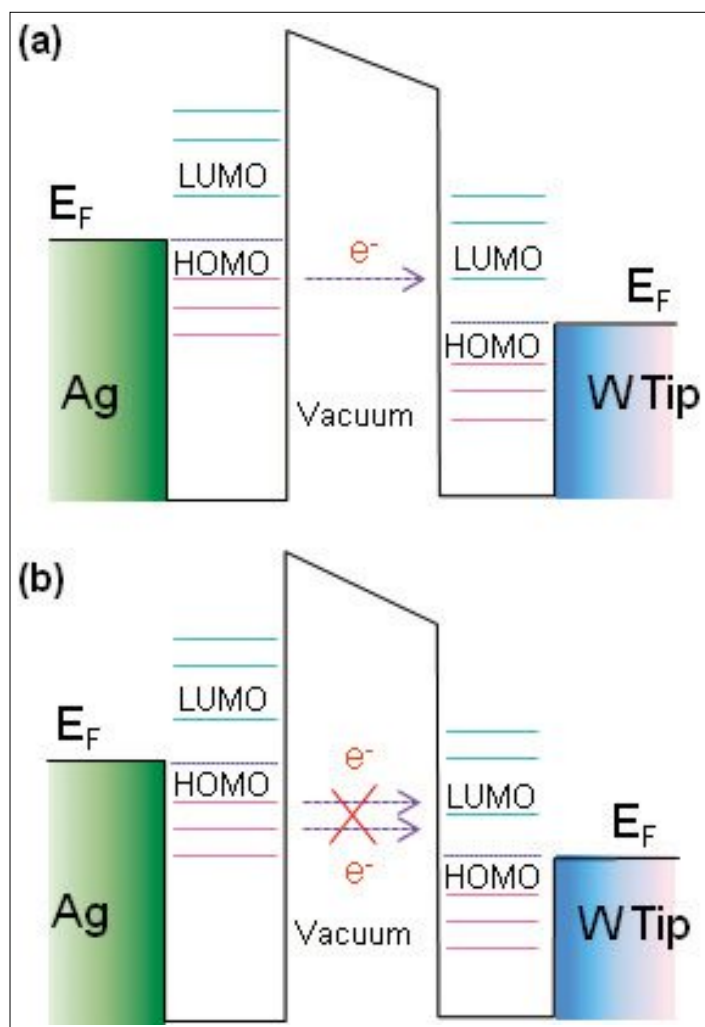

Fig. 7. Schematic drawing of one tunneling junction consisting of a molecule-terminal tip and a molecule-covered metal surface. The modified tip can discriminate the molecule states and electronic properties of the metal surface. (a) The highest occupied molecular orbital (HOMO) levels of the adsorbed molecules match the lowest occupied molecular orbital (LOMO) levels of the molecule at the tip apex within a certain voltage bias range, allowing molecule states to be imaged. (b) No orbital of the adsorbed molecule matches any orbital of the molecule at the tip apex, thus no states of the adsorbed molecule are visible.
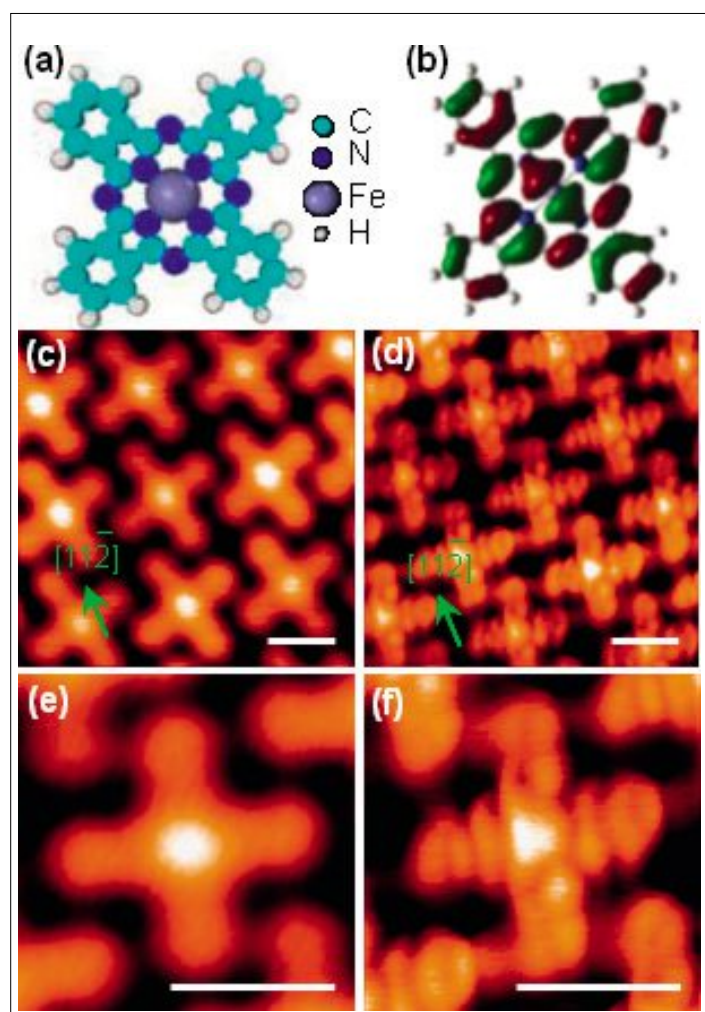
Fig. 8. Comparison of STM images of FePc monolayer on Au(111) surface probed by different tips. (a) Structure of FePc. (b) HOMO of an isolated FePc molecule. (c) and (e) are obtained with a bare metallic tip. (d) and (f) are obtained with a O₂-functionalized tip. All images are obtained with $U = -0.4$ V, $I = 0.05$ nA. Scale bar is 1 nm.
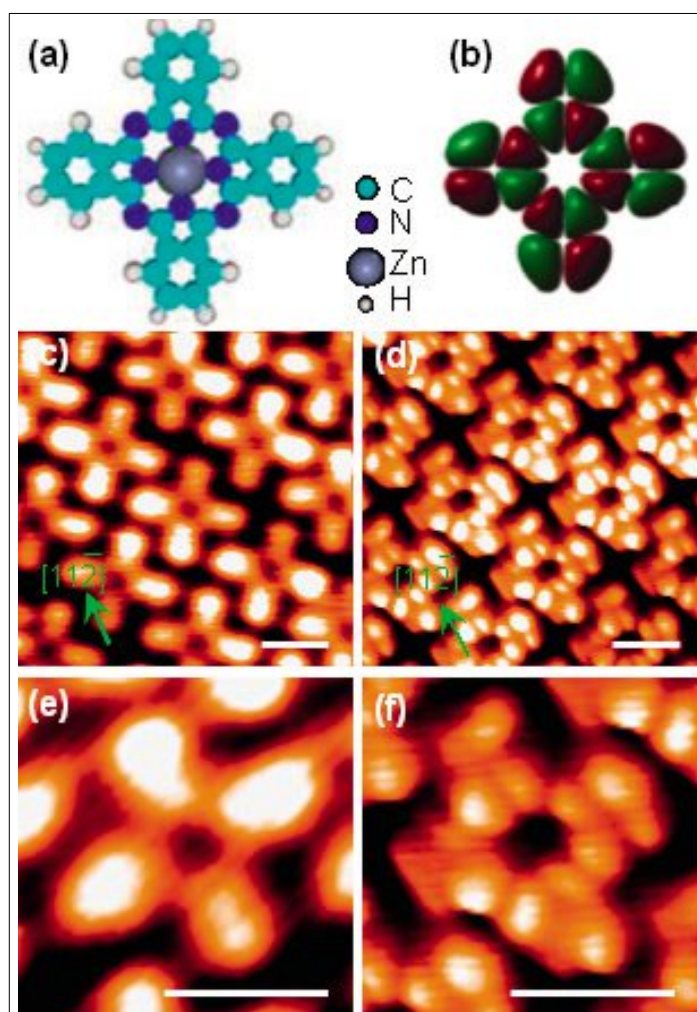
Fig. 9. STM topographic images of ZnPc monolayer on Au(111). (a) Structure of ZnPc. (b) HOMO of a free ZnPc molecule. (c) and (e) are obtained with a bare tungsten tip. (d) and (f) are obtained with a O₂-functionalized STM tip. Scanning parameters: $U = -1.6$ V, $I = 0.05$ nA. Scale bar: 1 nm.

calculation revealed that the π orbitals of the perylene molecule merge completely with the charge density of the metal surface, which therefore greatly changes the charge density of the clean tungsten tip. The functionality of this tip, *i.e.* the discrimination of perylene states, is therefore due to the mismatch of energy levels of perylene molecules on the Ag surface and on the modified STM tip. As illustrated by Fig. 7a, electron tunneling occurs only between electron levels with the same energy. Within a certain bias range the HOMO orbital level of the adsorbed molecule is equal to the LOMO orbital of the molecule at the tip apex, the electron can tunnel from the adsorbed molecule to the tip, and thus we see the molecule states. But with greater bias voltage (Fig. 7b), no electron tunnels from the adsorbed molecule to the tip because the HOMO orbital level of the adsorbed molecule does not match any LOMO orbitals of the molecule at the tip apex, we thus cannot see any states of the adsorbed molecule.

In short, we have shown that the elec-

tronic states of perylene adsorbates and Ag substrates can easily be disentangled by using a modified STM tip. The π states of the perylene adsorbate can be imaged with a clean tungsten tip. Functionalizing the tip by attaching a perylene molecule on its apex enables high-resolution images of the underlying Ag(110) surface states. This indicates that functionalizing STM tips with organic molecules can open up a new route for energy selection of transport properties through organic interfaces.

4. See Molecule Orbitals at a Metal Surface with an O₂-terminated Tip

Direct imaging of detailed molecular orbitals can provide a deeper understanding of the molecule–substrate interaction and reactions at a sub-molecular or even atomic scale. Besides solid molecules (like perylene described above), small gas molecules can also be used to functionalize a tip and detect molecular structures with higher resolution. In our experiments, elec-

tronic states of both iron phthalocyanine (FePc) and zinc phthalocyanine (ZnPc) molecules on Au(111) were directly imaged by an O₂-terminated tip,[49] however, the corresponding electronic structures are not observable with a normal metallic tip.

Both FePc and ZnPc are typical planar MPc molecules, composed of a flat Pc skeleton with an iron or zinc ion in the central cavity (see Fig. 8a and Fig. 9a). Highly ordered FePc or ZnPc monolayer can be self-assembled on Au(111) surface.[29,50,51] Fig. 8b shows a typical STM image of highly ordered FePc monolayer on Au(111) obtained by a normal tungsten STM tip. Each FePc molecule is recognized as a four-lobed 'cross' structure with a central round protrusion as illustrated in Fig. 8e. This indicates that the FePc molecules are in a flat-lying geometry on the terraces. The STM image of a highly ordered ZnPc monolayer is shown in Fig. 9c. The ZnPc molecules also have a flat-lying adsorption configuration, and they are quite similarly imaged as a four-lobed 'cross' pattern with a normal STM tip, but the central zinc atom

appears as a round hole as shown in Fig. 9e, unlike FePc, whose central iron atom appears as a protrusion. The FePc and ZnPc molecules show identical orientations on Au(111), with the 'cross' directed in the [1-10] and [11-2] directions of the Au(111) surface. The enhanced brightness at the center of FePc is ascribed to a large tunneling current that results from orbital-mediated tunneling through the half-filled d_{z^2} orbital of the Fe ion. In the case of ZnPc, the d orbitals of Zn are fully filled and there is no electronic state contributing to tunneling near the E_F.[52–54] Therefore the zinc ion of a ZnPc molecule appears as a hole in the STM images.

With an O_2-functionalized STM tip, both FePc and ZnPc molecules can be imaged with sub-molecular resolution (see Fig. 8d and Fig. 9d, respectively). Intramolecular features are revealed very well in the close-up STM images of FePc and ZnPc molecules, as presented in Fig. 8f and Fig. 9f. Comparing images obtained with a normal tip, the central protrusion of the FePc molecule appears as a nearly equilateral triangle when probed with the functionalized tip, while it appears as a featureless round bump in the image taken with the normal tip. The specific features are also observed within the molecular lobes. The features of lobes in different directions are different, similar to the highest occupied molecular orbital (HOMO) of a free FePc molecule, as shown in Fig. 8b. The triangular protrusion at the iron position is different from the HOMO of a free FePc molecule, demonstrating a strong effect of the substrate on the center iron.

As for the ZnPc molecule imaged with the functionalized tip, the round central depression remains, and the rest of the molecule is substantially better resolved than with a normal tip. Each of its four lobes shows similar intramolecular features, in which each lobe is divided into four small protrusions with different intensity. This is similar to the HOMO of an isolated ZnPc molecule (Fig. 9b). Unlike the FePc/Au(111) system in which the adsorption changes the center protrusion from round to triangular, the center of ZnPc is still a round hole after adsorption. This difference must be attributed to their different molecule–substrate interactions resulting from their different central metal ions, since the chemical structures of FePc and ZnPc are similar. The interaction between Fe^{2+} and the substrate is stronger than that of Zn^{2+} and the substrate.

In order to fully understand the physical information behind these high-resolution STM images, first-principles calculations were performed for the adsorption of FePc (and ZnPc) on Au(111). STM images were simulated using a realistic W(111) tip[55] (single-atom terminated pyramid,
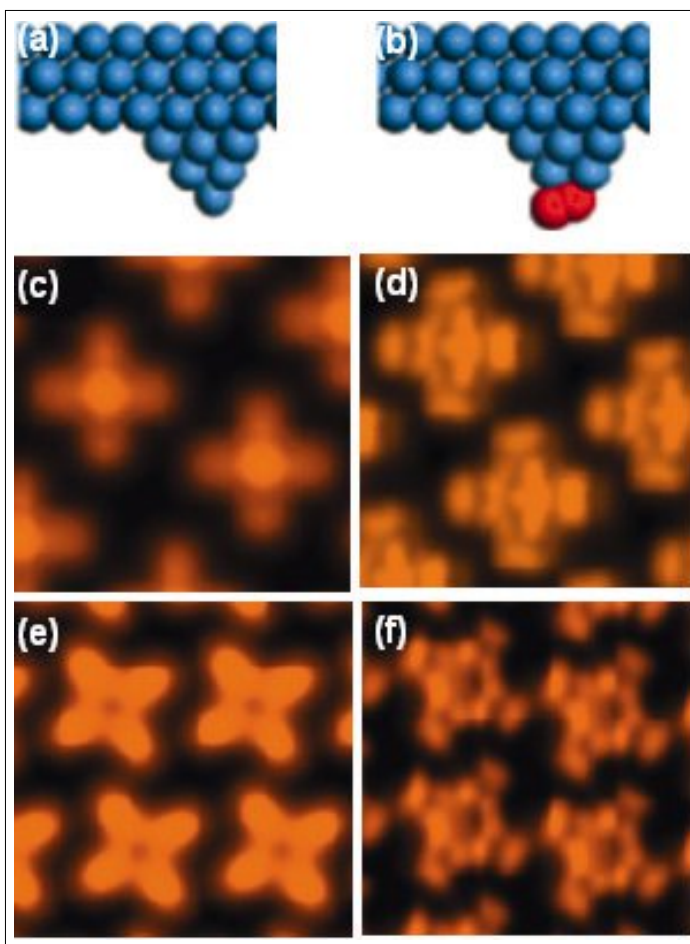

Fig. 10. Functionalization of a STM tip and its usage in exploring molecular electronic orbitals. (a) Side view of a normal W(111) tip apex supported by a W slab. (b) Side view of O_2 functionalized W(111) tip (red balls are oxygen atoms). (c)–(f) Simulated STM images using different tips: (c) FePc and (e) ZnPc on Au(111) simulated with a bare metallic STM tip; (d) FePc and (f) ZnPc on Au(111) simulated with an O_2-functionalized STM tip.

Fig. 10a) and a tip with one O_2 molecule attached to it (Fig. 10b). The simulation using the W(111)-oriented tip shows a four-lobed 'cross' structure with a round protrusion in the center for FePc/Au(111) (Fig. 10c), while a 'cross' structure with a round 'hole' in the center for ZnPc/Au(111) (Fig. 10e). The simulations using O_2-terminated tip show the intramolecular features within the FePc and ZnPc molecules (Fig. 10d and Fig. 10f, respectively). All simulations are in good agreement with the experimental results, especially the asymmetry inside each lobe of the molecular orbital resolved images. For the O_2 functionalized tip, we found that the oxygen atoms create a new localized electronic state near the Fermi level of the tip,[49] which should make the intramolecular features of HOMO of FePc and ZnPc molecules visible. The key difference between a clean tip and an O_2 functionalized tip turned out to be the energetic registry between tip orbitals and orbitals of the molecules at the surface.

5. Summary

We demonstrated that the technique of functionalizing a metal tip by sharpening or molecule-attaching could be a simple way to improve the resolution of STM. First, not only twelve adatoms but also six rest atoms in a unit cell of Si(111)-7×7 surface were resolved simultaneously with high contrast. The brightness of rest atom protrusions in STM topography is even comparable to the topmost adatoms within a certain bias range. The highest resolution topography with a visibility of rest atoms was ascribed to a very sharp tip, which was enunciated by first-principles simulations. Second, the electronic states of perylene adsorbates and Ag substrates can be discriminated by using a perylene-modified tip. High-resolution STM images of the surface states of the underlying Ag(110) lattice are obtained. Third, submolecular resolution STM images of FePc and ZnPc molecules on Au(111) are gained by using O_2-functionalized tips, by which intramolecular electronic features are observable. In the latter two cases, it turns out that the energy levels match between the molecule-terminated tip orbitals and orbitals of the molecule adsorbates at the surface. The experimental results are in excellent agreement with simulated STM images based on theoretical calculations.

[1] C. J. Chen, 'Introduction to Scanning Tunneling Microscopy', Oxford University Press, Oxford, **1993**.

[2] J. K. Gimzewski, C. Joachim, *Science* **1999**, *283*, 1683.

[3] C. Joachim, J. K. Gimzewski, A. Aviram, *Nature* **2000**, *408*, 541.

[4] H. J. Gao, K. Sohlberg, Z. Q. Xue, H. Y. Chen, S. M. Hou, L. P. Ma, X. W. Fang, S. J. Pang, S. J. Pennycook, *Phys. Rev. Lett.* **2000**, *84*, 1780.

[5] F. Rosei, M. Schunack, Y. Naitoh, P. Jiang, A. Gourdon, E. Laegsgaard, I. Stensgaard, C. Joachim, F. Besenbacher, *Prog. Surf. Sci.* **2003**, *71*, 95.

[6] M. Feng, X. F. Guo, X. Lin, X. B. He, W. Ji, S. X. Du, D. Q. Zhang, D. B. Zhu, H. J. Gao, *J. Am. Chem. Soc.* **2005**, *127*, 15338.

[7] W. Ji, Z. Y. Lu, H.-J. Gao, *Phys. Rev. Lett.* **2006**, *97*, 246101.

[8] M. Feng, L. Gao, Z. T. Deng, W. Ji, X. F. Guo, S. X. Du, D. X. Shi, D. Q. Zhang, D. B. Zhu, H. J. Gao, *J. Am. Chem. Soc.* **2007**, *129*, 2204.

[9] M. Feng, L. Gao, S. X. Du, Z. T. Deng, Z. H. Cheng, W. Ji, D. Q. Zhang, X. F. Guo, X. Lin, L. F. Chi, D. B. Zhu, H. Fuchs, H. J. Gao, *Adv. Funct. Mater.* **2007**, *17*, 770.

[10] J. V. Barth, G. Costantini, K. Kern, *Nature* **2005**, *437*, 671.

[11] H. J. Gao, L. Gao, *Prog. Surf. Sci.* **2010**, *85*, 28.

[12] B. Yang, Y. L. Wang, H. Y. Cun, S. X. Du, M. C. Xu, Y. Wang, K. H. Ernst, H. J. Gao, *J. Am. Chem. Soc.* **2010**, *132*, 10440.

[13] Y. L. Wang, S. Fabris, G. Costantini, K. Kern, *J. Phys. Chem. C* **2010**, *114*, 13020.

[14] N. Jiang, Y. L. Wang, Q. Liu, Y. Y. Zhang, Z. T. Deng, K. H. Ernst, H. J. Gao, *Phys. Chem. Chem. Phys.* **2010**, *12*, 1318.

[15] H. Y. Cun, Y. L. Wang, B. Yang, L. Zhang, S. X. Du, Y. Wang, K. H. Ernst, H. J. Gao, *Langmuir* **2010**, *26*, 3402.

[16] Y. Wang, M. Lingenfelder, T. Classen, G. Costantini, K. Kern, *J. Am. Chem. Soc.* **2007**, *129*, 15742.

[17] B. Yang, Y. L. Wang, G. Li, H. Y. Cun, Y. Ma, S. X. Du, M. C. Xu, Y. L. Song, H. J. Gao, *J. Phys. Chem. C* **2009**, *113*, 17590.

[18] S. L. Tait, Y. Wang, G. Costantini, N. Lin, A. Baraldi, F. Esch, L. Petaccia, S. Lizzit, K. Kern, *J. Am. Chem. Soc.* **2008**, *130*, 2108.

[19] T. Classen, M. Lingenfelder, Y. Wang, R. Chopra, C. Virojanadara, U. Starke, G. Costantini, G. Fratesi, S. Fabris, S. de Gironcoli, S. Baroni, S. Haq, R. Raval, K. Kern, *J. Phys. Chem. A* **2007**, *111*, 12589.

[20] Y. L. Wang, W. Ji, D. X. Shi, S. X. Du, C. Seidel, Y. G. Ma, H. J. Gao, L. F. Chi, H. Fuchs, *Phys. Rev. B* **2004**, *69*, 075408.

[21] D. X. Shi, W. Ji, X. Lin, X. B. He, J. C. Lian, L. Gao, J. M. Cai, H. Lin, S. X. Du, F. Lin, C. Seidel, L. F. Chi, W. A. Hofer, H. Fuchs, H. J. Gao, *Phys. Rev. Lett.* **2006**, *96*, 226101.

[22] B. C. Stipe, M. A. Rezaei, W. Ho, *Science* **1998**, *279*, 1907.

[23] J. K. Gimzewski, C. Joachim, R. R. Schlittler, V. Langlais, H. Tang, I. Johannsen, *Science* **1998**, *281*, 531.

[24] L. Gao, W. Ji, Y. B. Hu, Z. H. Cheng, Z. T. Deng, Q. Liu, N. Jiang, X. Lin, W. Guo, S. X. Du, W. A. Hofer, X. C. Xie, H. J. Gao, *Phys. Rev. Lett.* **2007**, *99*, 106402.

[25] L. Gao, Q. Liu, Y. Y. Zhang, N. Jiang, H. G. Zhang, Z. H. Cheng, W. F. Qiu, S. X. Du, Y. Q. Liu, W. A. Hofer, H. J. Gao, *Phys. Rev. Lett.* **2008**, *101*, 197209.

[26] Y. F. Wang, J. Kroger, R. Berndt, W. Hofer, *Angew. Chem. Int. Ed.* **2009**, *48*, 1261.

[27] J. Repp, G. Meyer, S. Paavilainen, F. E. Olsson, M. Persson, *Science* **2006**, *312*, 1196.

[28] J. Repp, G. Meyer, S. M. Stojkovic, A. Gourdon, C. Joachim, *Phys. Rev. Lett.* **2005**, *94*, 026803.

[29] Z. H. Cheng, S. X. Du, N. Jiang, Y. Y. Zhang, W. Guo, W. A. Hofer, H. J. Gao, *Surf. Sci.* **2011**, *605*, 415.

[30] D. M. Eigler, C. P. Lutz, W. E. Rudge, *Nature* **1991**, *352*, 600.

[31] L. Bartels, G. Meyer, K. H. Rieder, *Appl. Phys. Lett.* **1997**, *71*, 213.

[32] J. R. Hahn, W. Ho, *Phys. Rev. Lett.* **2001**, *87*, 196102.

[33] L. Bartels, G. Meyer, K. H. Rieder, *Surf. Sci.* **1999**, *432*, L621.

[34] G. Binnig, H. Rohrer, C. Gerber, E. Weibel, *Phys. Rev. Lett.* **1982**, *49*, 57.

[35] G. Binnig, H. Rohrer, C. Gerber, E. Weibel, *Phys. Rev. Lett.* **1983**, *50*, 120.

[36] P. Avouris, R. Wolkow, *Phys. Rev. B* **1989**, *39*, 5091.

[37] M. A. Lantz, H. J. Hug, P. J. A. van Schendel, R. Hoffmann, S. Martin, A. Baratoff, A. Abdurixit, H. J. Guntherodt, C. Gerber, *Phys. Rev. Lett.* **2000**, *84*, 2642.

[38] F. J. Giessibl, S. Hembacher, H. Bielefeldt, J. Mannhart, *Science* **2000**, *289*, 422.

[39] P. Sutter, P. Zahl, E. Sutter, J. E. Bernard, *Phys. Rev. Lett.* **2003**, *90*, 166101.

[40] K. Takayanagi, Y. Tanishiro, M. Takahashi, S. Takahashi, *J. Vac. Sci. Technol. A* **1985**, *3*, 1502.

[41] R. J. Hamers, R. M. Tromp, J. E. Demuth, *Phys. Rev. Lett.* **1986**, *56*, 1972.

[42] Y. L. Wang, H. J. Gao, H. M. Guo, H. W. Liu, I. G. Batyrev, W. E. McMahon, S. B. Zhang, *Phys. Rev. B* **2004**, *70*, 073312.

[43] Y. L. Wang, H. M. Guo, Z. H. Qin, H. F. Ma, H. J. Gao, *J. Nanomater.* **2008**, *2008*, 1.

[44] F. J. Giessibl, *Science* **1995**, *267*, 68.

[45] R. S. Becker, B. S. Swartzentruber, J. S. Vickers, T. Klitsner, *Phys. Rev. B* **1989**, *39*, 1633.

[46] R. Wiesendanger, 'Scanning probe microscopy and spectroscopy: methods and applications', Cambridge University Press, Cambridge, England, **1994**.

[47] L. Gao, Z. T. Deng, W. Ji, X. Lin, Z. H. Cheng, X. B. He, D. X. Shi, H. J. Gao, *Phys. Rev. B* **2006**, *73*, 075424.

[48] Z. T. Deng, H. Lin, W. Ji, L. Gao, X. Lin, Z. H. Cheng, X. B. He, J. L. Lu, D. X. Shi, W. A. Hofer, H. J. Gao, *Phys. Rev. Lett.* **2006**, *96*, 156010.

[49] Z. H. Cheng, S. X. Du, W. Guo, L. Gao, Z. T. Deng, N. Jiang, H. M. Guo, H. Tang, H. J. Gao, *Nano Research* **2011**, *4*, 523.

[50] Z. H. Cheng, L. Gao, Z. T. Deng, N. Jiang, Q. Liu, D. X. Shi, S. X. Du, H. M. Guo, H. J. Gao, *J. Phys. Chem. C* **2007**, *111*, 9240.

[51] Z. H. Cheng, L. Gao, Z. T. Deng, Q. Liu, N. Jiang, X. Lin, X. B. He, S. X. Du, H. J. Gao, *J. Phys. Chem. C* **2007**, *111*, 2656.

[52] X. Lu, K. W. Hipps, *J. Phys. Chem. B* **1997**, *101*, 5391.

[53] M. S. Liao, S. Scheiner, *J. Chem. Phys.* **2001**, *114*, 9780.

[54] S. Yoshimoto, E. Tsutsumi, K. Suto, Y. Honda, K. Itaya, *Chem. Phys.* **2005**, *319*, 147.

[55] A. S. Lucier, H. Mortensen, Y. Sun, P. Grutter, *Phys. Rev. B* **2005**, *72*, 235420.